Articles

Liquid-Feed Flame Spray Pyrolysis of Nanopowders in the Alumina−Titania System

Sanghak Kim,[†,‡] J. J. Gislason,[§] R. W. Morton,[§] X. Q. Pan,[†] H. P. Sun,[†] and R. M. Laine*[,†]

Department of Materials Science and Engineering, University of Michigan, Ann Arbor, Michigan 48109-2136, and ConocoPhillips Petroleum Co., 92E Bartlesville Technology Center, Bartlesville, Oklahoma 74004

Received February 17, 2004. Revised Manuscript Received March 31, 2004

We report here the synthesis of $(TiO_2)_x(Al_2O_3)_{1-x}$ nanopowders with molar ratios that span the $TiO_2-Al_2O_3$ composition range. The nanopowders were synthesized using liquid-feed flame spray pyrolysis (LF−FSP) of mixtures of $N(CH_2CH_2O)_3TiOiPr$ (titanatrane isopropoxide) and $N(CH_2CH_2O)_3Al$ (alumatrane) dissolved in the appropriate molar ratios in alcohols used as solvent and fuel. Ethanol, methanol, and butanol were used in an attempt to regulate the flame temperatures, particle sizes, and size distributions, as well as to influence the phase(s) produced in selected mixed-phase materials produced at $x = 0.5$. The as-produced powders were characterized in terms of phase, size, specific surface area, composition, and morphology by BET, XRD, SEM, TEM, and TGA−DTA. At compositions close to Al_2O_3, the δ phase is the primary phase observed. As the compositions approach $x = 0.5$, a combination of rutile, α-Al_2O_3, and Al_2TiO_5 is observed. Pure titania powders consist of 90:10 mixtures of anatase and rutile; however, doping with $x = 0.05$ of alumina results in 40:60 anatase/rutile mixtures and nearly pure rutile phase at $x = 0.15$. The source of this latter phase transformation can be explained in terms of Al^{3+} substituting for Ti^{4+} ions in the anatase lattice forcing the phase transformation as found in highly defective TiO_2. No effect of flame temperature as a function of fuel was observed.

Introduction

Ultrafine and nanosized single-metal oxide powders, especially fumed silica, titania, and alumina, are common commercial products generated in kiloton/year quantities. Until recently, it has been difficult to obtain ultrafine and nanosized mixed-metal oxide powders despite the clear need for such materials by both the commercial and academic communities. Furthermore, the potential to generate single- and multiphase ultrafine and nanosized materials adds further facets to the diverse potential opportunities that these materials hold.

We have previously described the use of liquid-feed flame spray pyrolysis (LF−FSP) as a means of producing nanosized oxide powders and benchmarked this process against titania and alumina.[1,2] These benchmark studies were followed by studies using LF−FSP to produce single-phase, mixed-metal nanopowders of β''-alumina[2] for alkali thermoelectric power electrolytes and $SrO{\cdot}Al_2O_3{\cdot}2SiO^3$ and $3Al_2O_3{\cdot}2SiO_2$ mullite glasses[4] for structural ceramic applications.[2−4]

Most recently, the LF−FSP process was used to produce $Y_3Al_5O_{12}$ composition nanopowders with a new phase for both structural and photonic applications.[5] Here, we begin studies targeting single- and multiphase mixed-metal oxide nanopowders.

Multiphase nanopowders are essentially ceramic/ceramic nanocomposites and are known to offer considerable potential for structural applications. For example, they are expected to be much tougher than traditional duplex ceramics, because crack propagation through nanocomposites must follow more torturous pathways than in micron-scale composites.[6−8] Furthermore, because nanosized powders can be pressed and sintered

* To whom correspondence should be addressed. E-mail: talsdad@umich.edu.
† University of Michigan.
‡ ConocoPhillips Petroleum Co.
§ On leave from Hyundai-Kia Motors Co.

(1) Bickmore, C. R.; Waldner, K. F.; Baranwal, R.; Hinklin, T.; Treadwell, D. R.; Laine, R. M. *J. Eur. Ceram. Soc.* **1998**, *18*, 287.
(2) Sutorik, A. C.; Neo, S. S.; Hinklin, T.; Baranwal, R.; Treadwell, D. R.; Narayanan, R.; Laine, R. M. *J. Am. Ceram. Soc.* **1998**, *81*, 1477.
(3) Laine, R. M.; Hinklin, T.; Williams, G.; Rand, S. C. *J. Met. Nano. Mat.* **2000**, *8*, 500.
(4) Baranwal, R.; Villar, M. P.; Garcia, R.; Laine, R. M. *J. Am. Ceram. Soc.* **2001**, *84*, 951.
(5) Marchal, J.; John, T.; Baranwal, R.; Hinklin, T.; Laine, R. M. *Chem. Mater.* **2004**, *16*, 822.
(6) Harmer, M. P.; Chan, H. M.; Miller, G. A. *J. Am. Ceram. Soc.* **1992**, *75*, 1715.
(7) Stearns, L. C.; Harmer, M. P. *J. Am. Ceram. Soc.* **1996**, *79*, 3013.

10.1021/cm0497531 CCC: $27.50 © 2004 American Chemical Society
Published on Web 05/19/2004

to transparency, they offer potential for the manufacture of structural and photonic materials for applications ranging from transparent armor[9] to new types of lasers.[10] Finally, multiphase mixed-metal oxide LF−FSP powders will have very high surface areas without microporosity, offering potential for catalyst applications.[11−14]

Heterogeneous catalysts often consist of multiple metals and metal oxides coated on other metal oxide supports, with alumina supports being very common.[12,13] In particular, photocatalysts have received considerable attention recently for applications ranging from direct conversion of light to electricity to self-cleaning, self-disinfecting surfaces.[14−17]

Titania is the primary material used in these applications because it absorbs the UV component (<340 nm) of solar radiation to generates holes and electrons that can be used directly to generate electricity.[14−17] Alternately, they also can be used to generate hydroxyl radicals and superoxide ions that react destructively with any organic in the immediate vicinity, leading to self-cleaning and self-disinfecting surfaces. Unfortunately, titania is relatively hydrophobic, making it poorly dispersible in water and thereby limiting its capacity to act as a photocatalyst. Consequently, titania is often modified with silica to improve its wetting behavior.[18] In contrast, nano-δ-alumina, made by the liquid-feed flame spray pyrolysis (LF−FSP) process, is highly hydrophilic and disperses very easily in water.[19]

Three older literature citations suggest that, under some conditions, titanium ions can be incorporated in the Al_2O_3 crystal lattice.[20,21] One report[20] describes a plasma method of producing these materials. TiO_2 is also known to form a metastable line compound with Al_2O_3 (Al_2TiO_5) that readily equilibrates with equivalent mixtures of α-Al_2O_3 and rutile.[21−24] All of these materials are potentially interesting from both catalyst support and photocatalyst perspectives.

Finally, recent reports by Lettman et al.,[15] Asahi et al.,[16] and Anpo et al.[17] point to the fact that incorporation of certain ions into the TiO_2 lattice changes the band gap such that these materials become photoactive at 400 nm. This is an exciting discovery because it suggests that more of the solar radiation envelope can be used for photocatalysis.

These points are the motivation for the efforts reported here to produce a series of alumina−titania compositions via LF−FSP as a starting point for the development of high-surface-area, highly hydrophilic nanocomposites for photocatalysts that operate at wavelengths ≤ 400 nm.

Experimental Section

Materials. Titanatrane isopropoxide or Tyzor TE was purchased from Dupont. Ethanol was purchased from standard sources and used as received. Alumatrane was prepared as described elsewhere.[25]

Precursor Preparation. A series of precursors corresponding to ceramic compositions $(TiO_2)_x(Al_2O_3)_{1-x}$ was prepared (x = 0.0, 0.16, 0.50, 0.65, 0.85, and 1.0). In all cases, alumatrane was used as the source of Al_2O_3, and titanatrane isopropoxide as the source of TiO_2. $N(CH_2CH_2O)_3Al$ has a density of 0.96 g/cm^3 and a ceramic content of 28.0 wt % Al_2O_3. An alumatrane/ethanol solution was prepared that contained 7 wt % Al_2O_3 as determined by TGA. The as-purchased titanatrane isopropoxide containing 20 wt % free ^{i}PrOH has a density of 0.99 g/cm^3 and a ceramic loading of 14.0 wt % TiO_2, as also confirmed by TGA.

Measured amounts of the two solutions were mixed in the appropriate amounts to make 500 mL of solutions of each of the precursor compositions listed above with the specified molar ratio, and then 2500 mL of EtOH was added with stirring at 20 °C. For experiments with other alcohols, the dilution was done with 2500 mL of MeOH or ^{n}BuOH. By changing the alcohol mixing ratio, it is possible to control the fuel content of the aerosol at constant flow rates and, in turn, the flame temperatures inside the chamber. The temperature differences inside the chamber (as expected) result in different quenching rates, thus affecting the final powder properties produced by LF−FSP.

LF−FSP Processing. The LF−FSP apparatus has been described in detail elsewhere.[1,2,25] Typically, a 2.5 wt % ceramic yield solution of precursor in an alcohol mixture is atomized at ∼30 mL/min in an ultrasonic atomizer with oxygen to generate an oxygen-rich aerosol that is ignited via methane/oxygen pilot torches in the device's ignition chamber. Combustion occurs at temperatures above 1500 °C, producing nanoscale titania−alumina powder and gaseous byproducts. A steep temperature gradient, >500 °C/s, between the combustion chamber and the 300 °C collection point (∼1.5 m) provides rapid quenching, as the powders are carried away from the combustion zone at velocities of <700 cfm using an inline radial pressure blower. The powders are collected downstream in a pair of 6-ft × 3-in. wire (alumel) in tube (Al) electrostatic precipitators (ESP) maintained at a 10 kV pseudo-dc potential. After completion of a run, the powders were recovered from the ESP tubes and stored in plastic bags in air.

Heat Treatment. Selected powders were annealed using a Thermolyne Type 6000 Furnace, equipped with a Eurotherm programmable temperature controller (model no. 818P, Northing, England).

Simultaneous Thermogravimetric and Differential Thermal Analysis. Phase transformations and mass loss events occurring during heating of as-prepared samples were investigated with a Simultaneous Differential Thermal (SDT)

(8) Hayashi, C., Uyeda, R., Tashki, A., Eds. *Ultra-fine Particles: Exploratory Science and Technology*; Noyes Publications: Westwood, NJ, 1997.
(9) U.S. Army Research Laboratory. *Transparent Armor Systems*; http://www.arl.mil/wmrd/Tech/TranspArmorSys.pdf.
(10) Gallas, M. R.; Hockey, B.; Pechenik, A.; Piermarini, G. J. *J. Am. Ceram. Soc.* **1994**, *77*, 2107.
(11) Moser, W. R., Ed. *Advanced Catalysts and Nanostructured Materials: Modern Synthetic Methods*; Academic Press: San Diego, CA, 1996.
(12) Nair, P.; Mizukami, F.; Okubo, T.; Nair, J.; Keizer, K.; Burggraaf, A. J. *Ceram. Process.* **1997**, *43*, 2710.
(13) Linacero, R.; Rojas-Cervantes, M. L.; Lopez-Gonzalez, J. De D. *J. Mater. Sci.* **2000**, *35*, 3279.
(14) Shklover, V.; Nazeeruddin, M. K.; Zakeeruddin, S. M.; Gratzel, M. *Chem. Mater.* **1997**, *9*, 430.
(15) Lettmann, C.; Heinrichs, H.; Maier, W. F. *Angew. Chem., Int. Ed.* **2001**, *40*, 3160.
(16) Asahi, R.; Morikawa, T.; Ohwaki, T.; Aoki, K.; Taga, Y. *Science* **2001**, *293*, 269.
(17) Anpo, M.; Kishiguchi, S.; Ichihashi, Y.; Takeuchi, M.; Yamashita, H.; Ikeue, K.; Morin, B.; Davidson, A.; Che, M. *Res. Chem. Intermed.* **2001**, *27*, 459.
(18) Stark, W. J.; Strobel, R.; Gunther, D.; Pratsinis, S. E.; Baiker, A. *Mater. Chem.* **2002**, *12*, 3620.
(19) Bell, N.; Rodriguez, M. Dispersion and processing of alumina nanopowders. *J. Nanosci. Nanotechnol.*, in press.
(20) Gani, M. S. J. McPherson, R. *J. Mater. Sci.* **1980**, *15*, 1915.
(21) Tanizaki, H.; Otsuka, A.; Niiyama, M.; Iwasaki, K. *Mater. Sci. Eng.* **1996**, *A215*, 157.
(22) Xiong, G.; Wang, X.; Lu, L.; Yang, X.; Xu, Y. *J. Solid State Chem.* **1998**, *141*, 70.
(23) Lee, H. L.; Lee, H. S. *J. Mater. Sci. Lett.* **1994**, *13*, 316.
(24) Jayaram, V. *Philos. Mag. A* **1988**, *57*, 525.
(25) (a) Laine, R. M.; Treadwell, D. R.; Mueller, B. L.; Bickmore, C. R.; Waldner, K. F.; Hinklin, T. *J. Chem. Mater.* **1996**, *6*, 1441. (b) Laine, R. M., Mueller, B. L., Hinklin, T. U.S. Patent 5,418,298, 1995.

Analyzer (TA Instruments, Inc., New Castle, DE). The transformation temperatures were determined by themogravimetric analysis were also measured using a model 2960 Simultaneous Thermogravimetric Analyzer. As-prepared powders of about 40 mg were hand pressed in a 3-mm dual-action die, placed inside Pt sample cups, and heated at ramp rates of 10 °C/min from room temperature to 1400 °C. The reference material was a pellet of α-alumina. A synthetic air flow of 50 mL/min was maintained during all SDT experiments. Precursor samples were placed in alumina sample cups with an empty alumina cup as the reference and heated at ramp rates of 5 °C/min to 1000 °C.

XRD Studies. As-prepared and calcined samples were characterized using (1) a Rigaku Rotating Anode Goniometer or (2) a Philips X′Pert Pro diffractometer. Powder samples for the Rigaku were prepared by placing ∼100 mg in XRD sample holders (amorphous silica slides) for data collection. Cu Kα (λ = 1.54 Å) radiation with a Ni filter was used with a working voltage and current of 40 kV and 100 mA, respectively. Scans were continuous from 10 to 80° 2θ with a step scan of 2° 2θ/min and increments of 0.05° 2θ. Peak positions and relative intensities were characterized by comparison with ICDD files for δ-, δ*-, θ-, and α-alumina (16-0394, 23-1009, 46-1215, and 10-0173, respectively). Peak positions and intensities for anatase, rutile, and Al_2TiO_5 were calculated using ICDD files 21-1272, 21-1276, and 26-0040, respectively.

XRD patterns taken on the Philips X′Pert Pro diffractometer used the following procedure:[26] Powders were packed in a 32-mm silicon metal low-background holder. These holders were used as a specimen to measure all background profiles. The diffractometer was equipped with a long, fine-focus copper X-ray source powered at 40 kV and 40 mA, an X′Celerator detector and beam tunnel, 0.04-rad source and receiving Soller collimators, a 20-mm source mask, a degree primary slit, and a degree anti-scatter slit.[27] Scans were acquired from 4° to 145° (2θ) with an increment of 0.05° (2θ) and a total acquisition time of 20 min [7.25° (2θ)/min]. Diffraction patterns were acquired using Philips Electronics Inc. Data Collector software and processed using Material Data, Inc.[28] Jade version 6.1 and Riqas version 4.0.0.8 software packages. Peak positions and relative intensities were characterized by comparison with ICDD files as above. A phase filter was prepared by including α-alumina, θ-alumina, δ-alumina, δ*-alumina, γ-alumina, anatase, rutile, TiC, and Al_2TiO_5 into a crystallographic library for Rietveld modeling.[29]

Scanning Electron Microscopy (SEM). A field-emission SEM instrument was used to image powder morphologies. Powder samples were prepared by ultrasonically dispersing the powder in distilled water. A drop of the suspension was placed on a carbon film on an aluminum microscope plate and allowed to dry. Powders were sputter coated with 10−40 nm of Au−Pd to reduce charging effects. An operating voltage of 5−30.0 kV was used.

Transmission Electron Microscopy (TEM). An analytical TEM instrument (model 2010F, JOEL, Osaka, Japan) was used to measure the particle size and morphology of as-prepared powders. Powder samples were prepared by dipping a holey carbon grid with tweezers into a vial of the as-prepared powder. The specimen was held in a Gatan double-tilt goniometer. An operating voltage of 200 kV was used.

FTIR Spectra. Transmission and diffuse reflectance Fourier transform (DRIFT) spectra were recorded on a Mattson Galaxy Series FTIR 3000 spectrometer (Mattson Instruments, Inc., Madison, WI). Optical-grade, random cuttings of KBr (International Crystal Laboratories, Garfield, NJ) were ground with 1.0 wt % of the sample to be analyzed. For DRIFT analysis, samples were packed firmly and leveled off at the upper edge to provide a smooth surface. For transmission IR measurements, 100 mg of each sample prepared for DRIFT analysis was pressed in a stainless steel double-action die (12.75-mm-diameter) at 100 MPa for 1 min in a Carver Laboratory Press (model 3912). The FTIR sample chamber was flushed continuously with N_2 prior to data acquisition in the range 4000−400 cm^{-1}.

Specific Surface Area (SSA) Measurements were obtained using a Micromeritics ASAP 2010 sorption analyzer. Samples (200 mg) were degassed at 400 °C/2 h. Each analysis was run at −196 °C (77 K) with nitrogen gas. The SSAs were determined by the BET multipoint method using at least five data points at relative pressures of 0.001−0.20.

Chemical Analyses were done by Galbraith Laboratories (Knoxville, TN).

Results and Discussion

The objectives of the current study are to develop structure−property−processing parameters for LF−FSP production of $(TiO_2)_x(Al_2O_3)_{1-x}$ mixed-phase oxide nanopowders with the objective of exploring the phase space that could be used to provide optimal photocatalytic activity with good-to-excellent wetting. The work reported here will provide the basis for developing doped systems based on the work of Lettman et al.[15] that will lead to photocatalytic activity at wavelengths of <400 nm.

Details of the FSP process have been published.[1,2] In previous papers, the complete characterizations of LF−FSP titania and alumina produced from titanatrane isopropoxide and alumatrane were described.[23,29] This earlier work serves as the foundation for the efforts reported here. Fortunately, these precursors are mutually soluble in a number of alcohol solvents, allowing mixtures of the two to be aerosolized and combusted using the LF−FSP process and thus providing access to high-specific-surface-area (SSA) nanopowders consisting of single-phase solid solutions and mixed-phase nanocomposites in the Al_2O_3−TiO_2 system.

Initial studies were done simply using EtOH as the solvent and fuel. However, in the Al_2O_3−TiO_2 phase diagram, the 50:50 composition, if heated above about 1400 °C, forms the metastable line compound Al_2TiO_5. Below this temperature, mixtures of Al_2TiO_5 with rutile and α-alumina are obtained. Thus, we sought to control the LF−FSP flame temperatures in an effort to determine whether different processing conditions could be used to produce pure Al_2TiO_5. Again, the goal was exploring the potential utility of this phase for photocatalytic activity. Below, we discuss the results of our efforts, beginning with powder characterization studies.

Powder Characterization. The LF−FSP $(TiO_2)_x$-$(Al_2O_3)_{1-x}$ powders were produced at rates of 15−20 g/h and were characterized by TEM, XRD, BET, and FTIR spectroscopy as follows.

Transmission Electron Microscopy (TEM). Micrographs of the $(TiO_2)_{16}(Al_2O_3)_{84}$ nanopowders (Figure 1) indicate that the majority of the powders are single crystals that are loosely aggregated and only rarely necked.

Digital diffraction studies (not shown) of these powders suggest a single phase (δ-alumina) with no evidence of a titania phase, although Rietveld refinement suggests that half the TiO_2 is present as the rutile phase; see below.

(26) Philips Analytical, P.O. Box 13, 7600 AA, Almelo, The Netherlands.

(27) The Gem Dugout, 1652 Princeton Drive, State College, PA 16803.

(28) Materials Data, Inc., 1224 Concannon Blvd., Livermore, CA 94550.

(29) *The Rietveld Method*; Young, R. A., Ed.; Oxford University Press: New York, 1997.

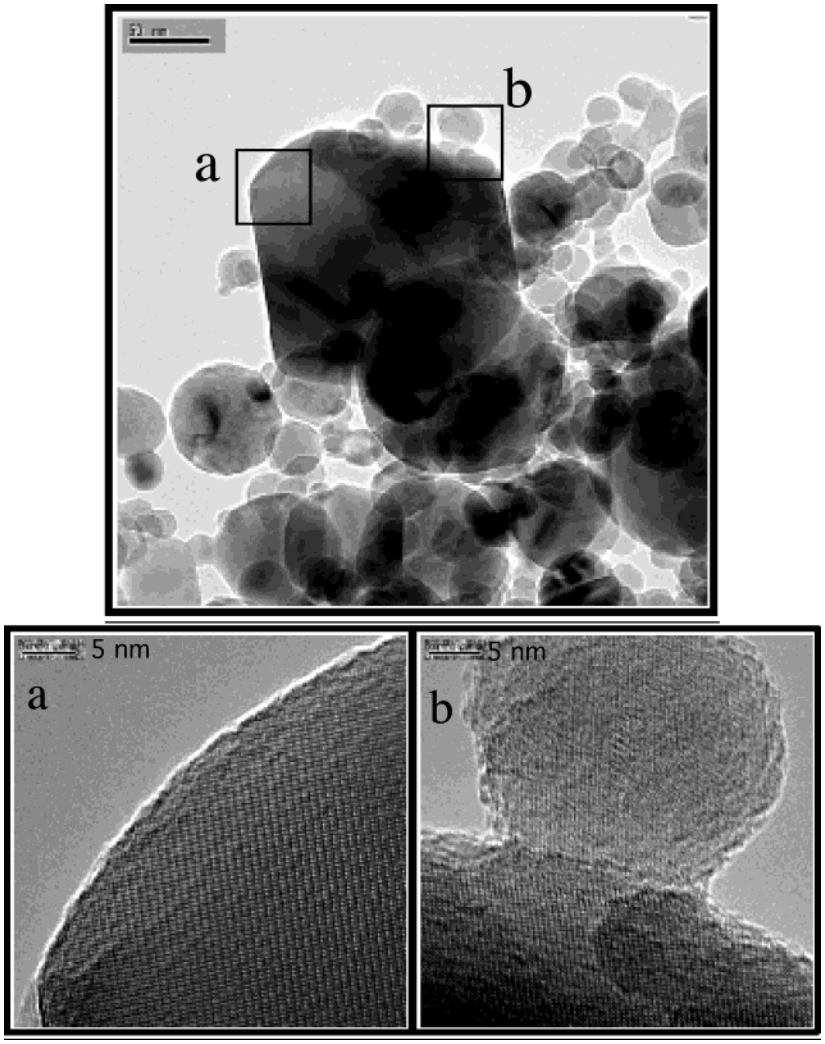

Figure 1. TEM images of $(TiO_2)_{16}(Al_2O_3)_{84}$ composition nanopowders with high-resolution images a and b.

Table 1. APSs (nm) of As-Prepared Powders Calculated from XRD Line Broadening, BET, and Rietveld Refinement

	composition				
	$x = 0$	$x = 0.16$	$x = 0.50$	$x = 0.65$	$x = 1$
XRD	23	21	18	21	42
BET	29	34	27	28	61
Rietveld	20	18	26		

BET Specific Surface Areas. The majority of the powders produced had SSAs of 40−60 m^2/g, which correspond to average particle sizes of 40−20 nm. There seems to be no specific conditions that provided much higher or much lower SSAs, even with different fuel mixtures. It should be noted that there is no evidence of microporosity, indicating that the powder particles are dense as formed; see the section on TEM characterization below. The BET-derived average particle sizes (APSs) and those from XRD line broadening and Rietveld refinement are reported in Table 1 and conform to average surface areas as expected.

XRD Patterns. The gross X-ray powder diffraction patterns of these powders are displayed in Figure 1; however, the very fine particle sizes of the $x \leq 0.5$ powders did not allow clear identification of their actual phase compositions. These materials were further studied by Rietveld refinement.

Some general observations can be made from the Figure 2 data. First, the end members, as noted above, were characterized previously with the phase composition of TiO_2 consisting of 90% anatase and 10% rutile. This is consistent with nano-titania produced by other gas-phase methods.[1] The pure Al_2O_3 powders are a 60:30 mix of δ- and γ-alumina, with the remaining 10% being θ-alumina. Possible reasons for δ- and γ-alumina forming rather than α-alumina, the thermodynamically favored phase at temperatures well below the typical LF−FSP flame temperatures (>1500 °C), are discussed in a previous paper.[30] The most likely explanation is that these phases are lower in density than α-alumina and phase transformations leading to lower surface/volume ratios will accommodate the very high surface energies in the resulting nanoparticles.

One surprising observation is that the addition of even small amounts of Al^{3+} to titania pushes the phase composition rapidly toward rutile such that, at only 0.15 mole percent Al^{3+}, almost pure rutile phase is favored over anatase. Possible reasons for this are discussed below.

Rietveld refinement permits more detailed characterization of the phases present in the nanopowders

(30) Hinklin, T.; Toury, B.; Gervais, C.; Babonneau, F.; Gislason, J. J.; Morton, R. W.; Laine, R. M. *Chem. Mater.* **2004**, *16*, 21.

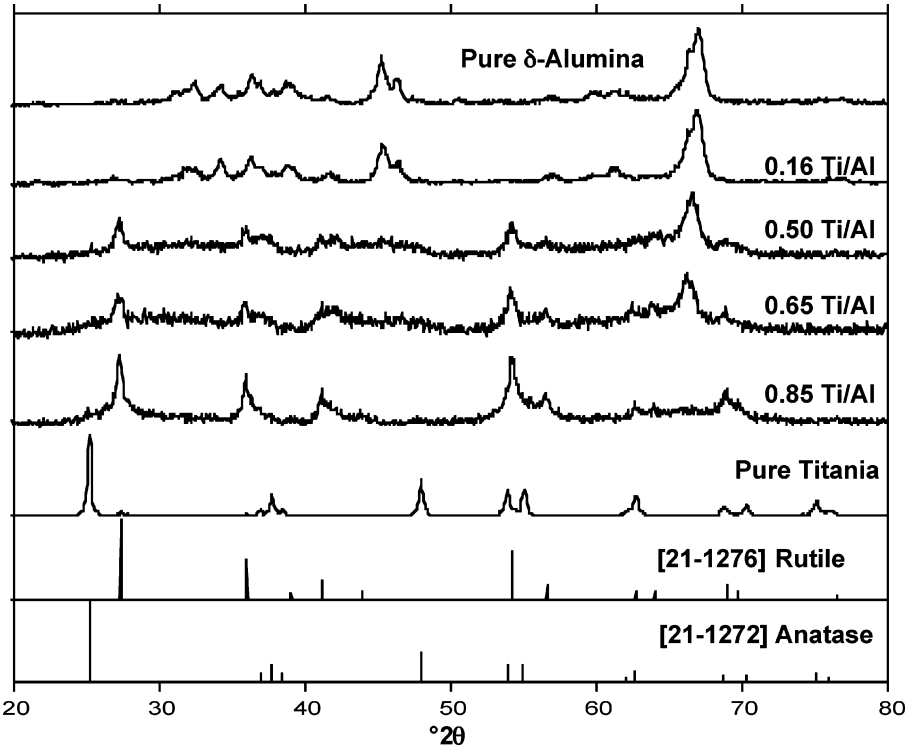

Figure 2. XRD patterns of as-prepared powders and standards.

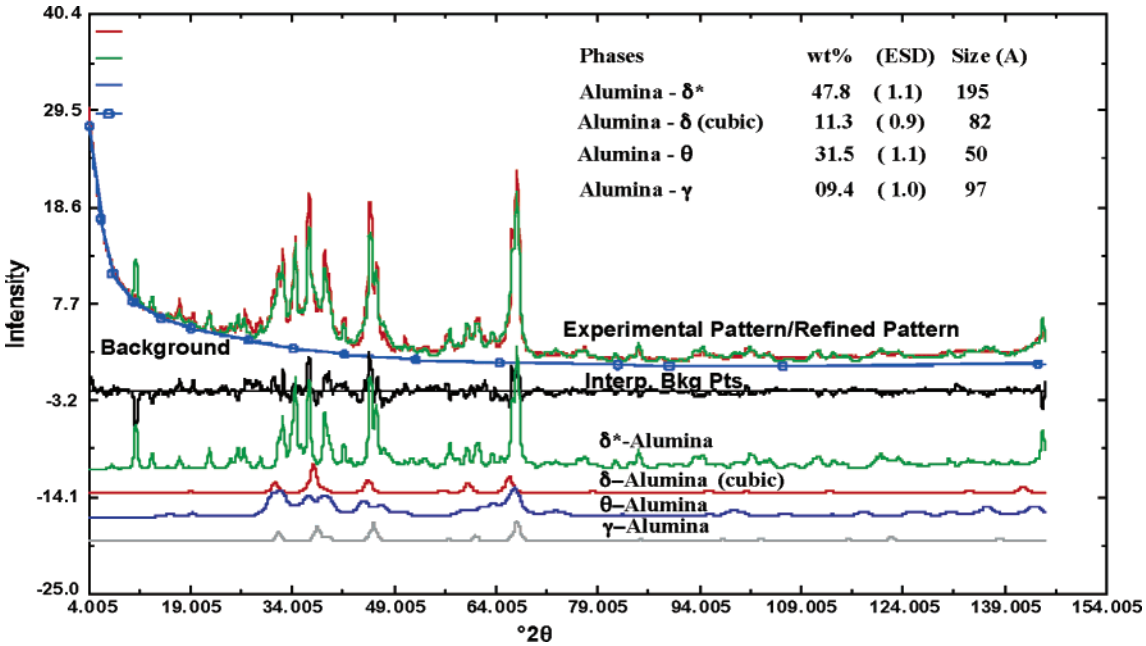

Figure 3. Rietveld refinement of alumatrane-derived Al_2O_3.

produced for $x < 0.5$. Figures 3 and 4 provide the Rietveld refinement data for the pure alumina powders ($x = 0$) as already reported and for the TiAl powders for $x = 0.16$.

Rietveld refinement uses published crystal structure data to calculate a theoretical XRD pattern so that the difference between the theoretical pattern and the measured pattern can be analyzed to obtain a better understanding of the structure of the particles. The data in Figure 3 are from an earlier paper[30] and not only demonstrate the utility in identifying the combination of phases produced but also provide a measure of the crystallite sizes for the various phases.

Thus, the major component is δ*-alumina with an average crystallite size that matches well with the Table 2 data. The data in Figure 4 suggest that the 16:84 materials are very similar, with typical particle sizes of the same order as the pure alumina materials. However, Rietveld refinement clearly indicates the presence of phase-separated rutile in these materials, which contradicts the earlier work in this area. The amount of phase-separated rutile is not consistent with the chemical analysis of these powders, which indicates that the composition produced is that used in the LF−FSP process. Hence, it is likely that a good portion of the remaining Ti^{4+} ions not accounted for by Rietveld

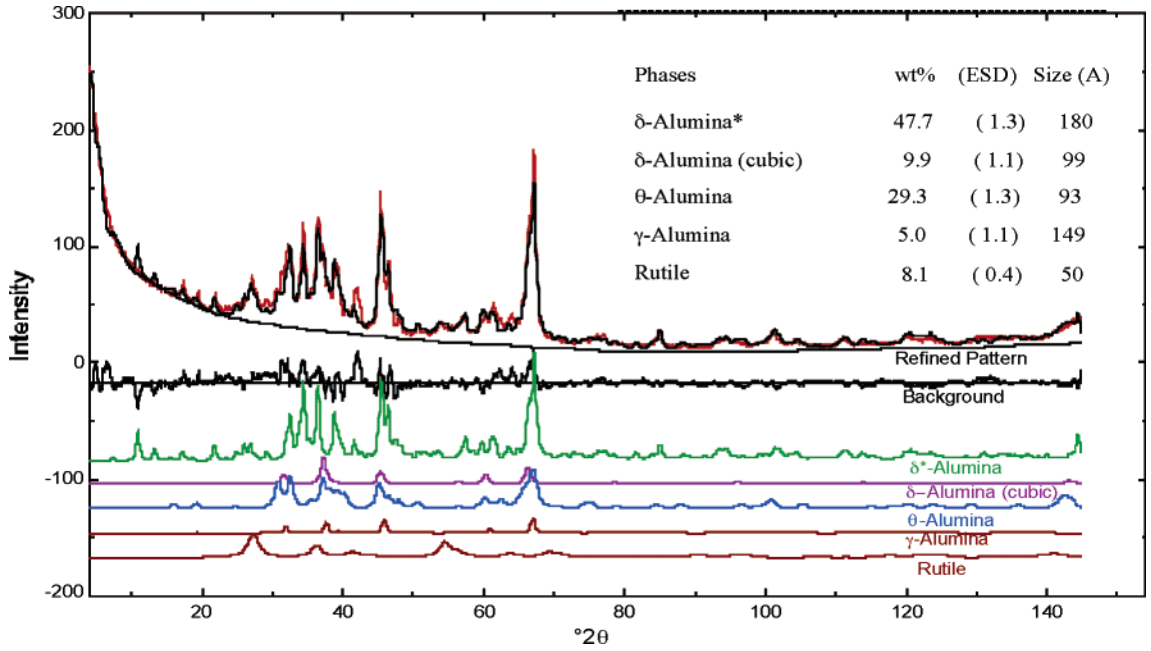

Figure 4. Rietveld refinement of 16:84 TiAl powders.

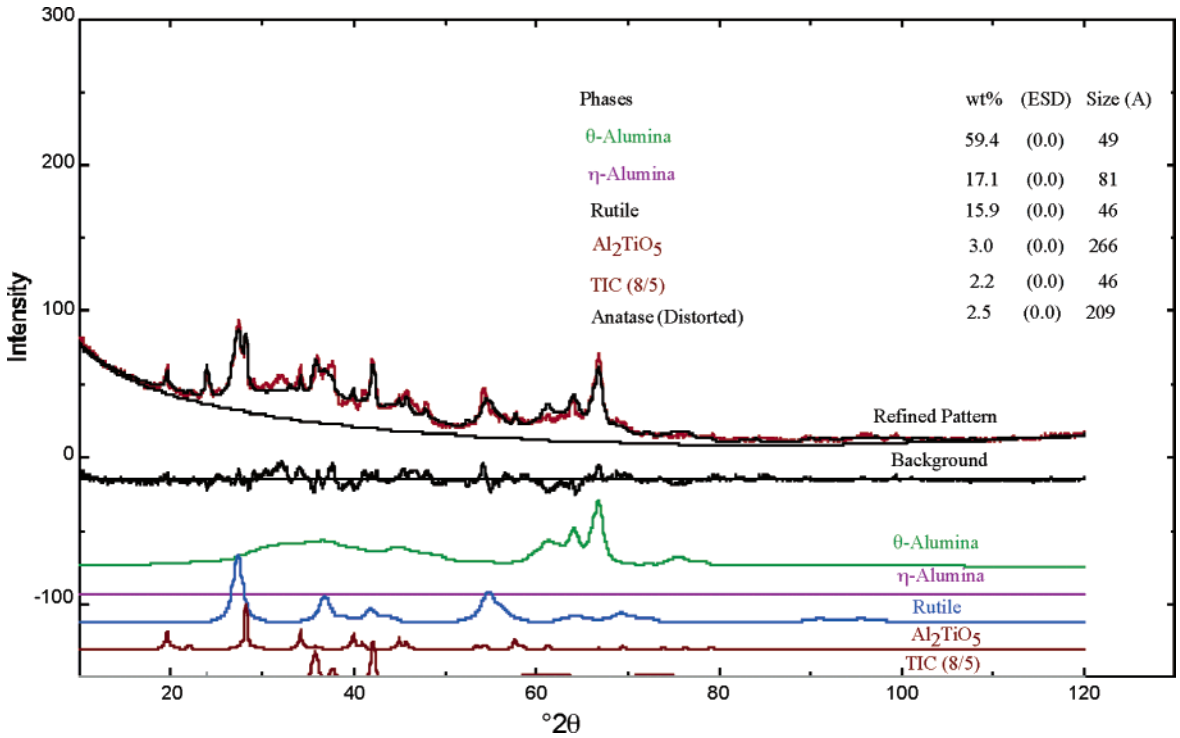

Figure 5. Rietveld refinement of 50:50 TiAl powders. Distorted anatase pattern not shown.

refinement most likely are present in the alumina lattice. Note that the accuracy of the phase compositions determined by Rietveld refinement can be ±3−5% for each weight percentage calculated.

The data in Figure 5 are at odds with what is known about the phase composition of the 50:50 mixtures, which suggest that Al_2TiO_5 is in equilibrium with α-alumina and rutile, rather than *θ*-alumina and rutile.[20−24] These results require further study. The suggested presence of TiC is also something that requires further study. TGA results, which would corroborate the presence of TiC, do not show any gain in mass with oxidation in air as would be expected.[31] However, this might be a consequence of the very slight amounts of TiC observed not providing sufficient mass changes to be observable.

Figure 6 records efforts to modify the phase composition of the 50:50 materials using MeOH to produce lower flame temperatures and ^{n}BuOH/EtOH to create higher flame temperatures. Pure ^{n}BuOH could not be used because the resulting flame temperatures are too high to be manageable in our LF−FSP system. Table 2

(31) Liu, Y.; Treadwell, D.; Kanisto, M.; Mueller, B. L.; Laine, R. M. *J. Am. Ceram. Soc.* **1997** *80*, 705.
(32) Chao, J.; Rossini, F. D. *J. Chem. Eng. Data* **1965**, *10* (4), 374.

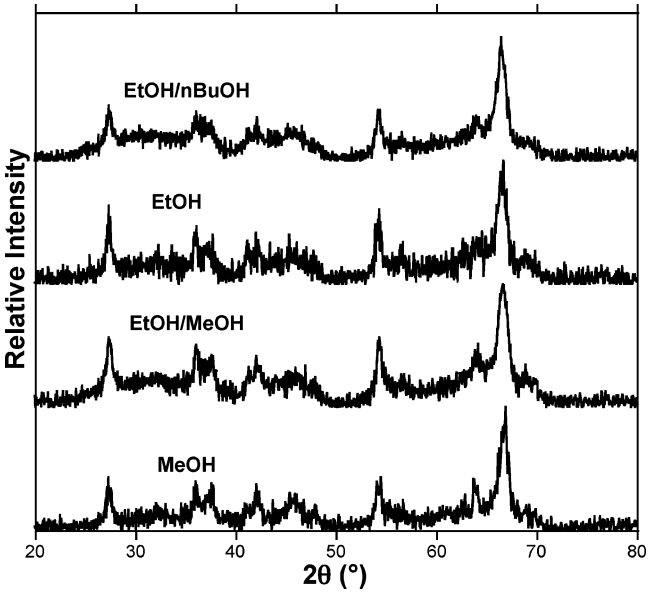

Figure 6. XRD patterns of $(TiO_2)_{0.5}(Al_2O_3)_{0.5}$ with variations of fuel composition. Volumetric ratio of mixed alcohol is 50:50 for each EtOH/^{n}BuOH and EtOH/MeOH.

Table 2. Heat of Combustion Data for Alcohol Fuels[32]

		heat of combustion $\Delta_c H°$		molecular weight	density
		(MJ/L)	(kJ/mol)	(g/mol)	(g/cm^3)
^{n}BuOH	($C_4H_{10}O$)	−29.3	−2677.4 ± 0.63	74.12	0.810
EtOH	(C_2H_6O)	−23.6	−1367.6 ± 0.3	46.07	0.795
MeOH	(CH_4O)	−17.9	−725.71 ± 0.13	32.04	0.791

reports the heat of combustion per unit volume of the alcohols used as fuels for LF−FSP. These data suggest that the flame temperatures should depend strongly on the ratio of the alcohols, from the lowest for MeOH to the highest for ^{n}BuOH.

The data in Figure 6 suggest that there are no gross differences between the materials formed with different apparent flame temperatures. This fact might suggest that it is the rapid quenching of the gas-phase-formed particles that determines the final phase composition of the powders. The TGA−DTA data do suggest some differences in the phase transformation temperatures upon heating but not sufficient to warrant further discussion. The particle sizes calculated from SSAs were all 16−20 nm.

Diffuse Reflectance IR Studies. Figure 7 provides diffuse reflectance infrared Fourier transform spectra (DRIFTS) of the as-produced powders. The region from 2000 to 4000 cm^{-1} is magnified 20× times to show a small band associated with νOH vibrations at >3500 cm^{-1} and trace νC−H bands at 2900−3000 cm^{-1}, suggesting some contamination by hydrocarbons. The νAl−O bands at 600 and 800 cm^{-1} are typical for these materials,[30] as is the band at 700 cm^{-1} for pure titania. The materials at 50:50 and 65:35 seem to be simple combinations of these bands, suggesting mostly segregated materials. Thus, there are no surprises from the FTIR data.

Phase Transformations on Heating. For pure TiO_2 powders, as-prepared powder XRD patterns show that anatase is the predominant phase, with rutile as the minor phase. The particle size determination using XRD line broadening shows APSs of ∼40 nm. After heat

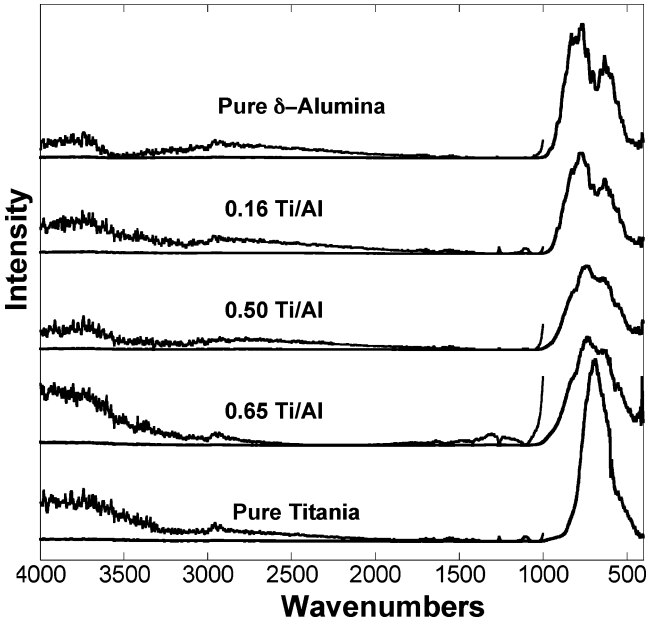

Figure 7. DRIFTS results for as-produced $(TiO_2)_x(Al_2O_3)_{1-x}$ powders, 1000−4000 cm^{-1} region 20×.

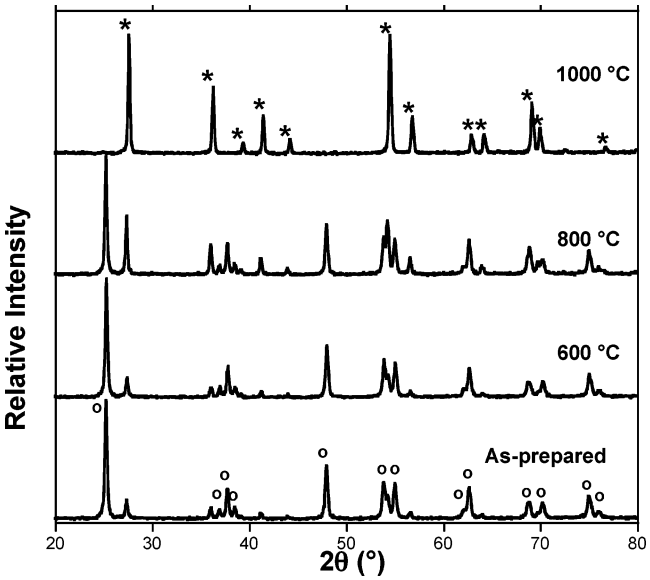

Figure 8. Phase transformation of pure titania powders (x = 1) heated at 10 °C/min with 0 h hold at temperature: ∗, rutile (21-1276); ○, anatase (21-1272).

treatment to 1200 °C at a ramp rate of 10 °C/min, the powders transform to the rutile phase (Figure 8).

The phase transformation data for LF−FSP TiO_2/Al_2O_3 are plotted in Figure 9. The various powders showed behavior similar to that observed in earlier work.[33−36] DTA scans (not shown) of the powders exhibit two exotherms above 1000 °C. An exotherm is seen first between 1050 and 1250 °C depending on composition, which was determined by XRD to be the δ- to α-alumina transformation. An endotherm thereafter at between 1340° and 1360 °C corresponds to the formation of

(33) Fargeot, D.; Mercurio, D.; Dauger, A. *Mater. Chem. Phys.* **1990**, *24*, 299.
(34) Gouma, P. I.; Mills, M. J. *J. Am. Ceram. Soc.* **2001**, *84*, 619.
(35) Francisco, M. S. P.; Mastelaro, V. R. *Chem. Mater.* **2002**, *14*, 2514.
(36) Bjorkert, U. S.; Mayappan, R.; Holland, D.; Lewis, M. H. *J. Eur. Ceram. Soc.* **1999**, *19*, 1847.

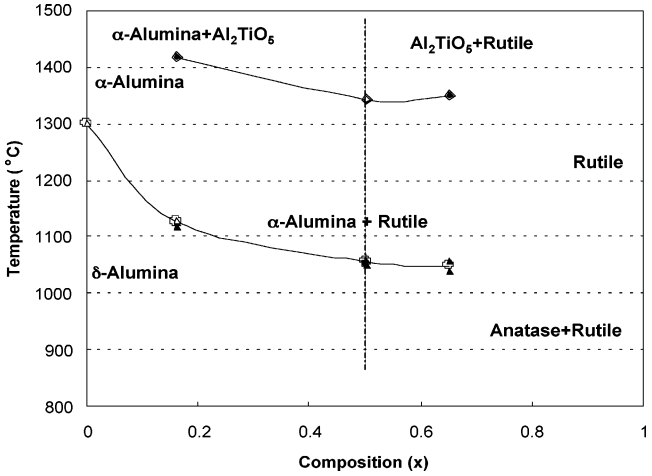

Figure 9. Phase transformation data for LF−FSP $(TiO_2)_x$-$(Al_2O_3)_{1-x}$. The lower line corresponds to the δ- to α-alumina transformation and the upper line to the formation of Al_2TiO_5.

Al_2TiO_5. The combined XRD and DTA data show that the anatase-to-rutile transformation occurs gradually between 700 and 1000 °C without a discernible peak.

$(TiO_2)_{0.85}(Al_2O_3)_{0.15}$. The observation of the pure rutile phase at this composition deserves some comment. Because Al^{3+} (0.53 Å) and Ti^{4+} lattice (0.61 Å) ions are of similar size and both favor octahedral oxygen coordination,[37] simple lattice substitution seems facile. The process is equivalent to introducing Ti^{3+} ions and must also generate oxygen vacancies, making the whole system highly defective. Several reports suggest that high defect densities will drive the anatase-to-rutile phase change.[20,22,37,38] Because the rutile phase is structurally denser than anatase, the oxygen vacancies appear to promote the transformation. It is important to note that the introduction of Al^{3+} might also change the band gap of the material relative to that of pure rutile. This is potentially important given our goal of creating materials that can function as photocatalysts at or near 400 nm.

In the same context, the band gap can also be adjusted by adding selected cations to the TiO_2 lattice.[15] The introduction of cations is also known to kinetically inhibit the anatase-to-rutile phase transformation.[39−41] Typically, ions larger than Ti^{4+}; such as Zn^{2+}, Co^{2+}, and Na^+, retard the transformation because it leads to a denser crystalline form. Surprisingly, however, even Al^{3+} was noted to inhibit the anatase-to-rutile phase transformation.[41,42] This effect was suggested to be a consequence of the segregation of alumina to the surface of titania particle.[38] In the LF−FSP system, this process does not seem to occur for this composition, but it is observed for the 1:1 system as noted above.

$(TiO_2)_{0.95}(Al_2O_3)_{0.05}$. In an effort to determine whether the extent of conversion to rutile could be controlled by the alumina content, we also produced a 5 mol % alumina doped sample and found that we were able to obtain a mixture that was approximately 60 mol % rutile and 40 mol % anatase. Again, this points to the potential for band gap manipulation. The literature also notes that the band gap can be modified (reduced) by introducing nitrogen to enhance photocatalytic activity.[16−18]

There now exist a set of tools for adjusting the TiO_2 band gap and therefore the photolytic activity. LF−FSP offers many opportunities to tune not only the band gap but also the wettability of the catalytic surface, thus offering the potential to develop and tailor optimal photocatalysts, especially those that are efficient at 400 nm.

Conclusions

To date, we have been able to prepare any composition desired in the $(TiO_2)_x(Al_2O_3)_{1-x}$ system. The resulting materials are very complex in phase composition and behavior. However, it appears possible to completely map compositions and phases in this system. In the range of $x = 1.0-0.85$, we can control the ratio of anatase/rutile phases from almost pure anatase to almost pure rutile. This type of controllability with LF−FSP processing is very useful for several applications. For example, photocatalytic properties might be affected by the phase mix, and the optimum composition or phase ratio can be investigated for the production of powerful photocatalyst using visible light instead of UV-light. In the range of $x = 0.65-0.50$, the phase mixes become more complex introducing alumina with the rutile phase. Alumina doping might affect the wettability and dispersibility of the titania photocatalyst because alumina has enhanced properties compared to titania in these two respects.

Acknowledgment. S.K. and R.M.L. thank the DSO National Laboratories of Singapore, Hyundai-Kia Motors Co., and in part AFOSR (F49620-03-1-0389) for support of this work.

CM0497531

(37) Akhar, M. K.; Pratsinis, S. E. *J. Mater. Res.* **1994**, *9*, 1241.
(38) Gesenhues, U. *Solid State Ionics* **1997**, *101−103*, 1171.
(39) Depero, L. E. Bontempi, E.; Sangaletti, L.; Notaro, M. *J. Mater. Res.* **2000**, *15*, 2080−6.
(40) Talavera, R. R.; Vargas, S.; Poniatowski, E. H. *J. Mater. Res.* **1997**, *12*, 439.
(41) Yang, J.; Ferreira, J. M. F. *Mater. Lett.* **1998**, *36*, 320.
(42) Hatta, K.; Higuchi, M.; Takahashi, J.; Kodaira, K. *J. Cryst. Growth* **1996**, *163*, 279.
(43) Shannon, R. D.; Pask, J. A. *J. Am. Ceram. Soc.* **1965**, *48*, 391.
(44) Hebrard, J.; Nortier, P. *J. Am. Ceram. Soc.* **1990**, *73*, 79.